Chemical Physics Letters 763 (2021) 138189

Contents lists available at ScienceDirect

Chemical Physics Letters

journal homepage: www.elsevier.com/locate/cplett

Research paper

Selection of interfacial metals for Si_3N_4 ceramics by the density functional theory

Sen Yang [a], Bingzheng Yang [a], Hao Ren [a], Huisheng Yang [a,*], Xiaolu Pang [a,*], Kewei Gao [a], Alex A. Volinsky [b]

[a] School of Materials Science and Engineering, University of Science and Technology Beijing, Beijing 100083, China
[b] Department of Mechanical Engineering, University of South Florida, Tampa 33620, USA

ARTICLE INFO

Keywords:
First principles
Interface
Work of separation
Electronic structure
Si_3N_4

ABSTRACT

Si_3N_4 has high mechanical strength and thermal cycling resistance, which can ensure reliability of electronic substrates under extreme environment. To enhance the wettability of ceramics and metal during the bonding process, it is necessary to use active metal. In this paper, charge density difference, density of sates and Bader charge of Si_3N_4 interfaces with Ti, Cr and Ni are respectively studied by first principles calculation. Results suggest that the electron transfer at the $Si_3N_4(11\bar{2}0)$/Ti(0001) interface is sufficient and the orbital hybridization of N and Ti is strong, indicating that it is the optimal interface between Si_3N_4 ceramics and metals.

1. Introduction

Ceramics substrate with high thermal conductivity, low coefficient of thermal expansion (CTE), and excellent heat and chemical resistance are used for high power module applications [1–3]. With the integration and miniaturization of electronic equipment, it is necessary to have higher power density and carry higher voltage and current on the premise of smaller size of electronic devices. In the near future, replacing Si with wide band gap semiconductor (SiC) will accelerate this trend [4–7]. However, as the power of the device increases, the thermal stress during service also increases, which requires the ceramic substrate to have excellent heat dissipation and thermal conductivity. Copper (Cu) metallization is usually used for various ceramic substrates, such as Al_2O_3, AlN and BeO. High temperature and large temperature difference ΔT during the working process will lead to device damage [8–9]. The high thermal stress caused by the CTE difference between copper and ceramics (such as Al_2O_3 or AlN) can lead to copper layer delamination [10–11], brings great safety risks to the stable equipment operation.

The electronic industry urgently needs to find high thermal conductivity substrate materials with good mechanical properties, so people begin to pay attention to Si_3N_4 ceramics. Si_3N_4 has three crystal structure, which are α phase, β phase and γ phase. Among them, α phase and β phase are the most common morphology of Si_3N_4, both of which are hexagonal structure [12]. Among the insulating ceramic materials, Si_3N_4 ceramics have many excellent properties, such as high hardness, high strength, small thermal expansion coefficient, good oxidation resistance and low friction coefficient, which is one of the ceramic materials with the best comprehensive mechanical properties [13]. For a long time, it is generally believed that Si_3N_4 ceramics do not have high thermal conductivity. The thermal conductivity of products such as Si_3N_4 bearing balls and structural parts is generally only 15–30 Wm^{-1} K^{-1}. Until 1995, Haggerty et al. calculated that the thermal conductivity of silicon nitride crystal could reach 320 Wm^{-1} K^{-1} according to the classical solid-state transport theory [14]. After that, Hirosaki et al. [15] calculated the thermal conductivity of a-axis and c-axis of β-Si_3N_4 by molecular dynamics method, which were 170 Wm^{-1} K^{-1} and 450 Wm^{-1} K^{-1}, respectively. In addition, the thermal expansion coefficient of Si_3N_4 is about 3.0×10^{-6}/℃, which matches well with the semiconductor chip materials such as SiC and GaAs. Such an expectation has fascinated many researchers to improve thermal conductivities of Si_3N_4 ceramics by a variety of means in recent years [16,17]. At present, the thermal conductivity of Si_3N_4 can be increased to 177 Wm^{-1} K^{-1} by reaction sintering silicon nitride(SRBSN) method [7], which is equivalent to AlN high thermal conductivity material, but the fracture toughness of Si_3N_4 prepared by this method is 11.2 MPa m1/2, which is three times of the latter. Based on this, more and more researchers set out to study the thermal cycle stability of Si_3N_4 ceramics metallized after thermal cycling.

It is difficult to connect Si_3N_4 and metal, and active filler metal is needed to improve the wettability of interface substrate [18–21,19–22].

* Corresponding authors.
E-mail addresses: hsyang@263.net (H. Yang), pangxl@mater.ustb.edu.cn (X. Pang).

https://doi.org/10.1016/j.cplett.2020.138189
Received 31 July 2020; Received in revised form 11 October 2020; Accepted 10 November 2020
Available online 14 November 2020

The commonly used methods include magnetron sputtering, laser cladding, and active metal brazing (AMB) [22–25]. The good combination between active metal and ceramic substrate directly affects the service life of high-performance electronic products [23–24]. It is reported that Si_3N_4 AMB substrate has excellent thermal cycling resistance [4,10,16,25]. Funaki et al. [16] have shown that the heat dissipation performance of copper plated Si_3N_4 substrate is equivalent to that of traditional high thermal conductivity ceramic AlN, and has excellent thermal cycling performance. Miyazakia et al. found that the thermal cycle reliability of Si_3N_4 AMB substrate is better than that of AlN AMB substrate under the same copper layer thickness and thermal cycle conditions [26]. Goets et al [27]. observed the Si_3N_4 AMB substrate after 6400 thermal cycles (-55℃~150℃) using acoustic emission scanning microscope (ASM), and found no internal cracks. In summary, Si_3N_4 AMB substrate will not delaminate after long-term storage at high temperature and thermal cycling in a wide temperature range, but it will lead to the decrease of shear strength and surface coarsening of the metal layer. However, there are some limitations in the observation of interface behavior and cracking. The delamination can be observed by optical microscope, but the initiation and propagation of microcracks under the delamination may be omitted [25]. It is difficult to independently study various similar factors and effects by relying on experimental methods. Therefore, it is extremely difficult to accurately evaluate the interface performance and bonding mechanism of active metals and Si_3N_4 ceramics.

In view of these limitations, physical modeling and theoretical calculation based on first principles at the electronic atomic scale have been gradually applied to the basic research on material interface as a relatively new means [28–30]. We have studied the stability and structure of ceramic metal interface by first principles [31]. At present, quite a number of first principles calculations have been successfully applied to metal ceramic interfaces, such as Al/nitride (VN, CrN, TiN), AlN/metal (al, Cu, Ti, Zr) systems. However, there are few studies on the binding properties of Si_3N_4 with active metals (Cr, Ti, Ni) at the atomic level and interface structure. The effects of microstructure and charge distribution on the interfacial properties of Si_3N_4 interfaces need to be further studied.

In this paper, the first principle calculations are used to construct interfaces composed of a series of low-index crystal surfaces of Si_3N_4 ceramics and Ti, Cr, Ni metals. By comparing the work of separation at the interface, several groups of interfaces with high bond strength are selected. In this paper the interface atomic and electronic structures are constructed to explain the microscopic mechanisms that affect the adhesion properties of the metal-ceramic interface, providing reasonable guidance and predictions on material selection and reliability assessment.

2. Methodology and calculation details

Energy and electronic structure calculations were performed using the Vienna ab initio simulation package [32–33], based on the density functional theory [34–35]. The exchange–correlation energy was treated in the framework of the generalized gradient approximation with the Perdew-Burke-Ernzerhof exchange [36–37]. The energy calculations were conducted in the Brillouin zone integrations based on the Monkhost–Pack grid [38]. Specifically, the k-point grids are set to $3 \times 3 \times 3$, $4 \times 4 \times 2$, $4 \times 4 \times 4$, and $5 \times 5 \times 5$, for the bulk phases Si_3N_4, Ti, Cr, and Ni, according to the convergence tests. The plane-wave cutoff energy can be finally set to 400 eV after the convergence test to ensure the accuracy and efficiency of the calculation results. The total energy calculation in this work is performed at T = 0 K, and the relaxation of the atomic position is achieved by the quasi-Newton (RMM-DIIS) algorithm for force minimization until the average force per atom was reduced to 0.02 eV/Å. An energy convergence criterion of 10_{-5}eV and 12 Å vacuum layer was used throughout the study.

Bulk properties were first evaluated for the accuracy of the adopted parameters. The surface of the material should be thick enough to ensure the accuracy of the calculations. More atomic layers result in bulk-like behavior but consume computing resources and time. For these parameters, the final choice was achieved through a series of convergence tests. Specific information is listed in Table 1, demonstrating that the employed theoretical calculations are pretty accurate, and the calculated data are reliable.

Table 1
Information about the models.

Parameter name	Parameter value	Selection reason
K-point grids	Si_3N_4: 3 × 3 × 3 Ti: 4 × 4 × 2 Cr: 4 × 4 × 4 Ni: 5 × 5 × 5	Convergence test
Number of surface layers	Si_3N_4(0001): 7 layers Ti(0001): 6 layers Cr(1 1 0): 7 layers Ni(1 1 1): 5 layers	Convergence test
Lattice parameter	Calculated value: β-Si_3N_4:a = b = 7.61700 Å, c = 2.91340 Å α-Ti: a = b = 2.9506 Å, c = 4.6788 Å Cr: a = b = c = 2.8846 Å Ni: a = b = c = 3.524 Å	References [39–42] Si_3N_4:a = b = 7.65 Å,c = 2.93 Å [39] Ti: a = b = 2.951 Å,c = 4.679 Å [40] Cr: a = b = c = 2.884 Å [41] Ni: a = b = c = 3.570 Å [42]

Table 2
The calculated surface energy of the main low index crystal planes of Si_3N_4, Ti, Cr, and Ni.

System	Structure	Orientation	Surface Energy, J/m^2
β-Si_3N_4	hcp	(0001)	3.0515
		$(10\bar{1}0)$	4.1684
		$(11\bar{2}0)$	3.9382
α-Ti	hcp	(0001)	2.0398
		$(10\bar{1}0)$	2.3000
		$(11\bar{2}0)$	1.9903
Cr	bcc	(1 0 0)	3.8477
		(1 1 0)	3.3656
		(1 1 1)	4.0123
Ni	fcc	(1 0 0)	2.2449
		(1 1 0)	2.3711
		(1 1 1)	1.9637

3. Results and discussion

3.1. Surface properties

Typically, the surface of the material has exposed grains, and the orientation of each grain may be different. In general, those crystal consist of the low index and low surface energy is the main part of the interface. Before constructing the interface model, the surface energy of the low index crystals needs to be calculated to compare and analyze the stability of the surface model. The surface energy (σsur) is commonly defined as the energy per unit area required to form a new surface and can be used to describe surface stability [43–44]. It is usually calculated according to the following formula [45–46]:

$$\sigma_{sur} = \frac{E_{slab}(N) - NE_{bulk}}{2A_s} \quad (1)$$

Here, $E_{slab}(N)$ is the total energy per surface of the slab, N is the total number of atoms in the slab, E_{bulk} is the bulk energy per atom in the bulk material, A_s is the area of the corresponding slab surface, and the factor of 2 indicates the presence of two identical surfaces of the slab.

The surface energy calculation results for Si_3N_4 ceramics and Ti, Cr,

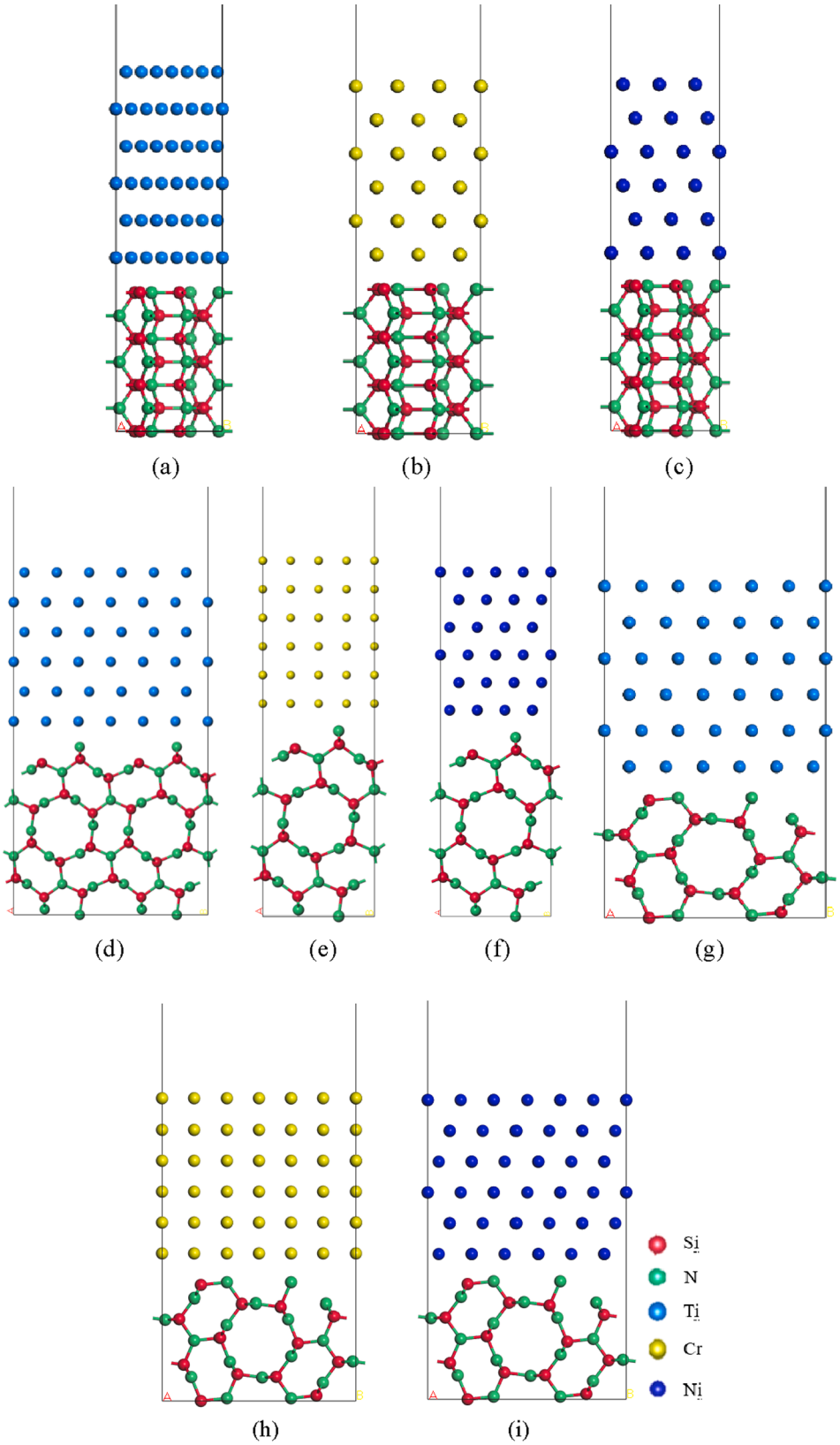

Fig. 1. Interface structures of (a) Si_3N_4(0001)/Ti (0001), (b) Si_3N_4 (0001)/Cr(1 1 0), (c) Si_3N_4 (0001)/Ni(1 1 1), (d) Si_3N_4 (10$\bar{2}$0)/Ti(0001), (e) Si_3N_4 (10$\bar{1}$0)/Cr(1 1 0), (f) Si3N4(10$\bar{1}$0)/Ni(1 1 1), (g) Si_3N_4 (1 1 $\bar{2}$0)/Ti(0001), (h) Si_3N_4 (1 1 $\bar{2}$0)/Cr (1 1 0), (i) Si_3N_4 (1 1 $\bar{2}$0)/Ni(1 1 1). (Cambridge blue: titanium; yellow: chromium; mazarine: nickel; green: nitrogen; red: silicon). (For interpretation of the references to color in this figure legend, the reader is referred to the web version of this article.)

and Ni metals low index crystal faces are listed in Table 2. Si_3N_4(0001), Ti(1 1 $\bar{2}$0), Cr(1 1 0) and Ni(1 1 1) crystal planes have the lowest surface energy of 3.05 J/m^2, 1.99 J/m^2, 3.36 J/m^2, and 1.96 J/m^2, respectively, indicating that these surface models have higher stability. The surface atoms in the crystal have dangling bonds and the number of atoms of different crystal faces is different, so the number of dangling bonds is also different. The density of atoms on the dense surface of the crystal is the largest, and the number of interactions between any atom on the surface and the atoms on the adjacent crystal face is the least. Therefore, when the dense surface is used, the number of dangling bonds is the

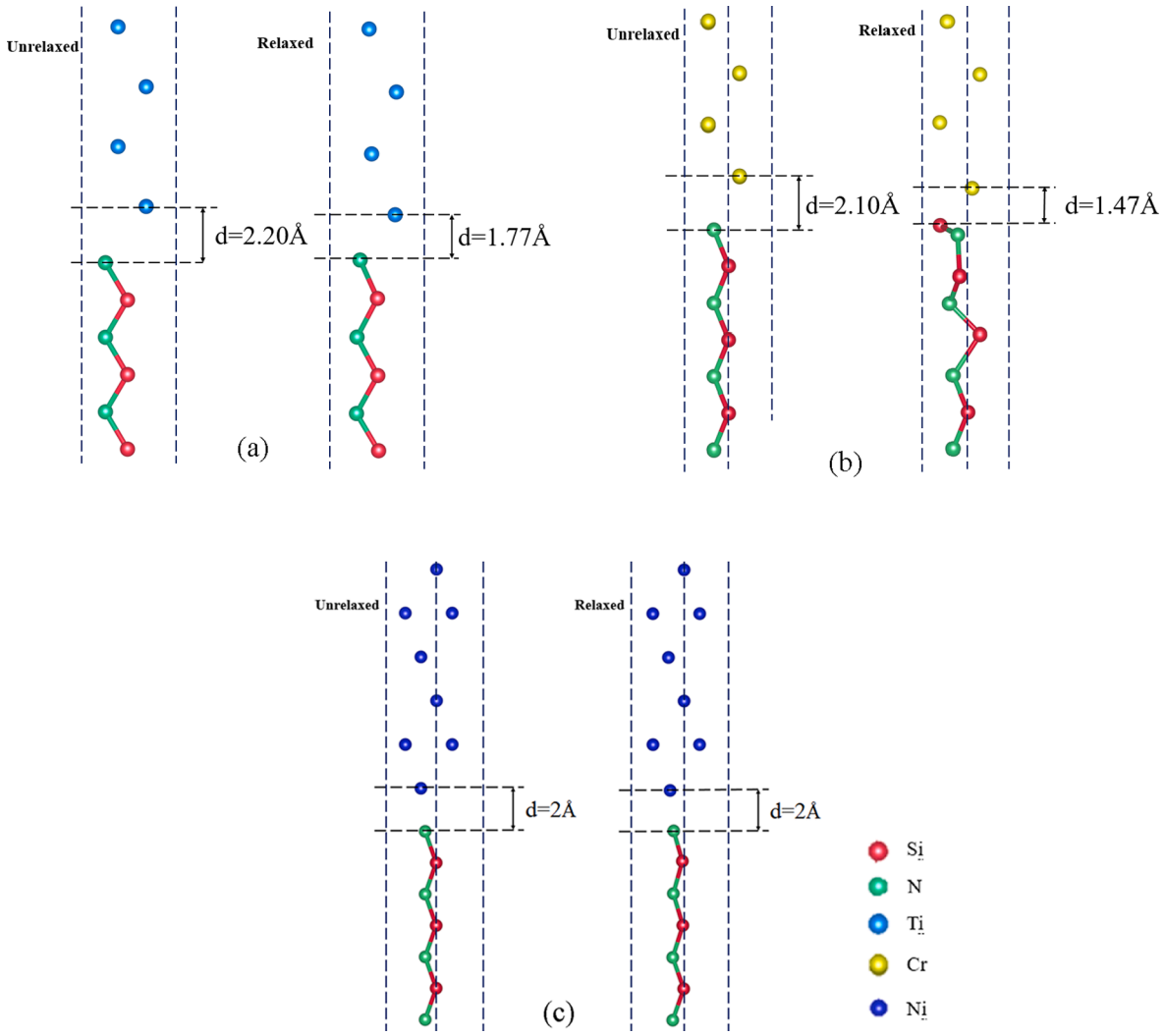

Fig. 2. Unrelaxed and relaxed atomic structures of. (a) Si_3N_4(0001)/Ti(0001) interface, (b) Si_3N_4(0001)/Cr(1 1 0) interface, (c) Si_3N_4(0001)/Ni(1 1 1) interface.

smallest, and the surface energy is the lowest. It is calculated that the surface energy of (1 1 $\bar{2}$0) Ti is slightly lower than the (0001) plane of the close-packed surface, but only by 0.04 eV. In the calculation process, the relaxation of atomic position is not considered, which may lead to errors up to several percent [47–48]. Therefore, we estimate that the combined error of the current surface energy is about 2%, which is related to the accurate density functional theory calculation.

3.2. Interface structure

The interfacial distance (d_0) greatly affects bonding between the interface atoms when constructing the interface model. Thus, choosing an appropriate interfacial distance is crucial for the stability of the constructed model. According to the previous literature results [49–50], 1.5–2 Å was selected for d_0.

There is a heterogeneous interface between metals and ceramics, and the lattice constants are quite different. When constructing the interface, one surface will be compressed or stretched to match the arrangement of atoms on the other surface. Generally, the soft metal surface is selected for stretching or compression, and its expansion ratio is called lattice mismatch degree. The interfacial mismatch was estimated by using the following parameter [51],

$$\text{mismatch} = \frac{b_\alpha - b_\beta}{b_\alpha} \tag{3}$$

where b is the lateral size of the slab, and subscripts α and β denote the components consisting of the interface, respectively. Generally speaking, when the lattice mismatch of the interface is less than 5%, the energy change caused by the lattice mismatch can be ignored [52–53]. In order to achieve a mismatch of less than 5%, the metal surface of the interface is also stretched or compressed (different orientation interfaces use different adjustment methods). The interface models were constructed for the main low index crystal faces of Si_3N_4 and Ti, Cr and Ni metals, as shown in Fig. 1.

3.3. Interface atomic relaxation

Structural relaxation refers to the adjustment of the coordinates of the entire input system to obtain a relatively stable ground state structure. In order to study the changes of atoms at the interface before and after structural optimization, the interfacial atomic relaxation of Si_3N_4(0001)/Ti(0001), Si_3N_4(0001)/Cr(1 1 0), and Si_3N_4(0001)/Ni (1 1 1) interfaces was studied.

Fig. 2. shows that the atomic geometry of relaxed interfaces undergoes a slight change, and the degree of atomic remodeling of the interface layers is small, so only the first layer near the interface changes. This can be reasonably explained by the lattice mismatch and interface distance of the initial configuration, so the initial interface structure is in a relatively stable state.

Table 3
The work of separation of the Si_3N_4/Ti interface with the main crystal orientation.

Ceramic Surface Orientation	Metal Surface Orientation	W_{sep}
Si_3N_4	Ti	J/m^2
(0001)	(0001)	3.06
	(10$\bar{1}$0)	3.34
	(11$\bar{2}$0)	—
(10$\bar{1}$0)	(0001)	3.29
	(10$\bar{1}$0)	3.23
	(11$\bar{2}$0)	—
(11$\bar{2}$0)	(0001)	5.45
	(10$\bar{1}$0)	4.92
	(11$\bar{2}$0)	—

Table 4
The work of separation of the Si_3N_4/Cr interface with the main crystal orientation.

Ceramic Surface Orientation	Metal Surface Orientation	W_{sep}
Si_3N_4	Cr	J/m^2
(0001)	(1 0 0)	—
	(1 1 0)	3.46
	(1 1 1)	2.05
(10$\bar{1}$0)	(1 0 0)	2.96
	(1 1 0)	2.93
	(1 1 1)	1.92]
(11$\bar{2}$0)	(1 0 0)	3.86
	(1 1 0)	4.01
	(1 1 1)	—

Table 5
The work of separation of the Si_3N_4/Ni interface with the main crystal orientation.

Ceramic Surface Orientation	Metal Surface Orientation	W_{sep}
Si_3N_4	Ni	J/m^2
(0001)	(1 0 0)	2.27
	(1 1 0)	—
	(1 1 1)	2.46
(10$\bar{1}$0)	(1 0 0)	2.63
	(1 1 0)	2.54
	(1 1 1)	2.6
(11$\bar{2}$0)	(1 0 0)	3.09
	(1 1 0)	2.84
	(1 1 1)	3.23

3.4. Work of separation

The ideal work of separation (W_{sep}) is the key quantity to predict the stability and adhesion properties of interfaces [54]. It is defined as the interface bond energy (per unit area) needed to separate the interface into two free surfaces, ignoring plastic deformation and atomic diffusion between the interfaces. It can be written as [55–56]:

$$W_{sep} = \frac{E_{slab,\alpha} + E_{slab,\beta} - E_{int}}{A_s} \quad (3)$$

Here, A_s is the interface area of the unit cell, $E_{slab,\alpha}$ and $E_{slab,\beta}$ denote the total energy of isolated α and β slabs, respectively. E_{int} is the total energy of the interface system.

Tables 3-5 list the work of separation in the interface models of the main low index crystal planes consisting of Si_3N_4, Ti, Cr, and Ni, respectively. The results show that the systems have larger work of separation in a series of low-index crystal interfaces. In the calculation of the previous surface model, the close-packed surface has the smallest surface energy, which indicates that the close-packed surface is the most stable. At the same time, the calculation results of the work of separation

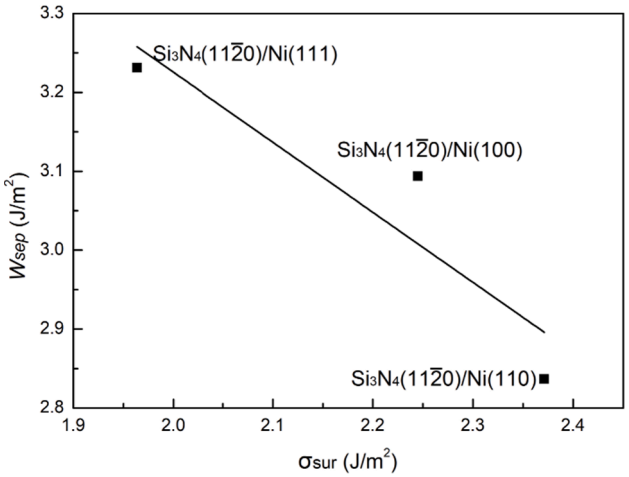

Fig. 3. The work of separation of the corresponding interface system and the surface energy of Ni low index crystal face.

of Si_3N_4 and Ti, Cr, and Ni show that the interface with the largest work of separation appears in a series of interface systems composed of close-packed surfaces. Therefore, to study the local interface structure and bonding, the following section of the paper will mainly discuss the Si_3N_4(1 1 $\bar{2}$0)/Ti(0001), Si_3N_4(1 1 $\bar{2}$0)/Cr(1 1 0) and Si_3N_4(1 1 $\bar{2}$0)/Ni (1 1 1) interfaces.

In order to further study the relationship between the surface energy and interfacial work of separation, the surfaces of Si_3N_4(1 1 $\bar{2}$0) and Ni (1 0 0), (1 1 0), (1 1 1) were selected. The surface energy σ_{sur} of the three low index crystal surfaces of Ni is plotted on the abscissa, and the ordinate is composed of interfacial separation W_{sep} in Fig. 3. The work of separation of the interface system decreases accompanied by the surface energy increase of the low-index crystal face of Ni. The results show that for metals, crystal surfaces with low surface energy should be selected to construct the interface model for higher bond strength and better interface stability.

3.5. Electronic structure and bonding

Fig. 4. (a), (b) and (c) show the charge density difference of the Si_3N_4(1 1 $\bar{2}$0)/Ti(0001), Si_3N_4(1 1 $\bar{2}$0)/Cr(1 1 0) and Si_3N_4(1 1 $\bar{2}$0)/Ni (1 1 1) interfaces, respectively. The dashed lines indicate the location of the interfaces. Red and blue areas represent charge increase and decrease, respectively. The electron density around Ti, Cr, and Ni atoms is reduced, and the electron density around the Si atom is also reduced accordingly. This indicates that electron transfer occurs at the interface of the three systems. Ti, Cr, and Ni with dangling bonds at the interface, respectively, form a chemical bond with N atoms, and electrons are biased around non-metallic N atoms. At the same time, the non-metallicity of N atoms in Si_3N_4 is stronger than Si atoms, so the electron density shifts towards N atoms and the electron density around Si atoms decreases accordingly. In addition, comparing the charge density difference of Si_3N_4 ceramics with three different metals, the charge transfer amounts at the three interfaces are significantly different. The atomic relaxation at the Si_3N_4(1 1 $\bar{2}$0)/Ti(0001) interface is sufficient, and the electron transfer between the Ti and the N atoms is more efficient, which is consistent with the previous calculation results of the work of separation and the interface energy. This preliminarily indicated that a stronger and more stable interface bonding system is formed between Si_3N_4(1 1 $\bar{2}$0)/Ti(0001).

The charge density difference only qualitatively reflects the electron transfer at the interface and the atomic bonding. In order to quantitatively represent the electron transfer and distribution between the interface atoms, the Bader charge of the interface atom is calculated. We

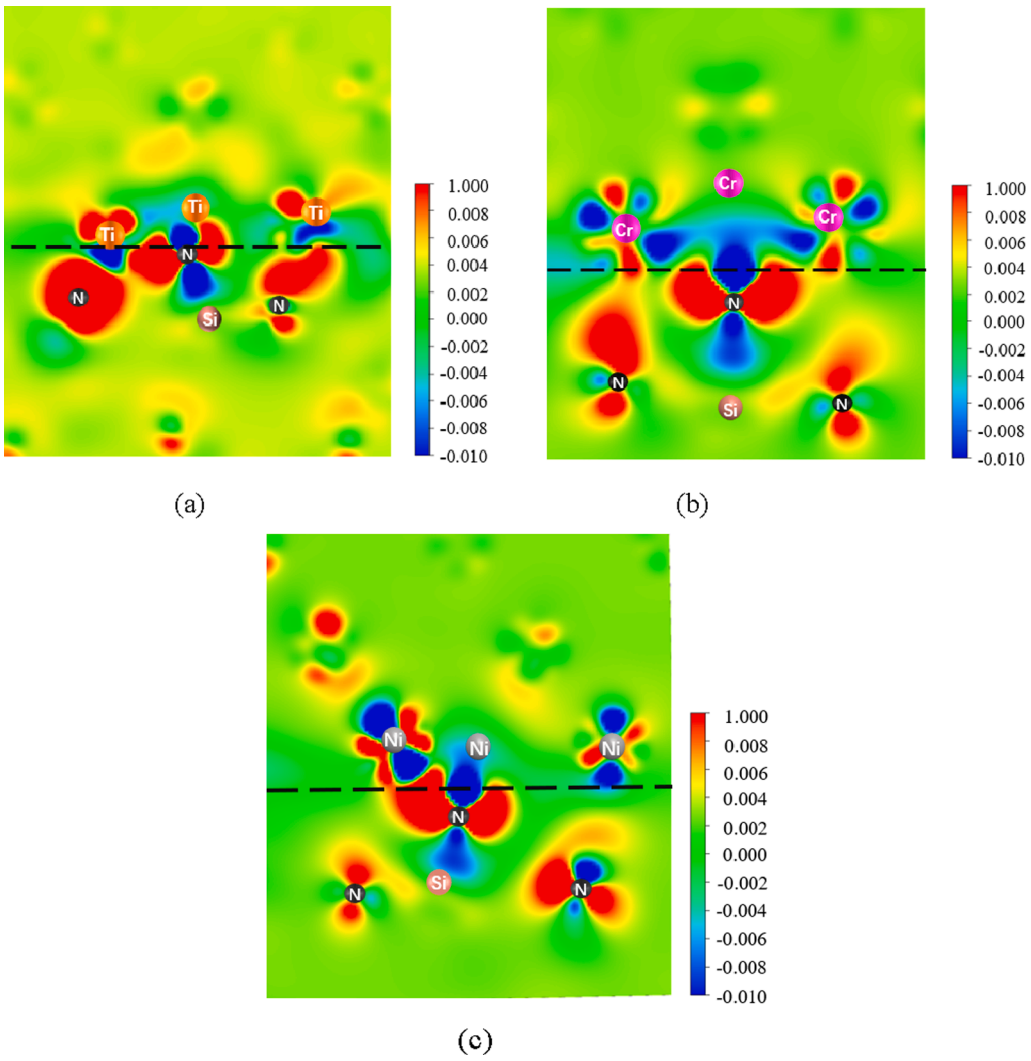

Fig. 4. Charge density difference of interface systems: (a) $Si_3N_4(11\bar{2}0)/Ti(0001)$, (b) $Si_3N_4(11\bar{2}0)/Cr(110)$, (c) $Si_3N_4(11\bar{2}0)/Ni(111)$.

Table 6
The Bader charge of interface systems.

Interface	Element	Valence electrons charge (e)	Atomic charge (e)	Charge Transfer (e)
$Si_3N_4(11\bar{2}0)/Ti$ (0001)	N	5	6.53	1.53
	Ti	4	3.64	−0.36
$Si_3N_4(11\bar{2}0)/Cr$ (110)	N	5	6.36	1.36
	Cr	6	5.42	−0.58
$Si_3N_4(11\bar{2}0)/Ni$ (111)	N	5	6.15	1.15
	Ni	10	9.56	−0.44

selected interfacial atoms, including N, Ti, Cr, and Ni, in order to look more closely at the Bader charge. Table 6 lists the charges at the $Si_3N_4(11\bar{2}0)/Ti(0001)$, $Si_3N_4(11\bar{2}0)/Cr(110)$, and $Si_3N_4(11\bar{2}0)/Ni(111)$ interfaces. In Table 6, the N atom on the Si_3N_4 side form an N-Si bond with one Si atom, and the other two unpaired electrons form a chemical bond with the metal atom. The electrons at the interface are transferred from the metal side to the Si_3N_4 ceramic side. The N atom of the $Si_3N_4(11\bar{2}0)/Ti(0001)$, $Si_3N_4(11\bar{2}0)/Cr(110)$ and $Si_3N_4(11\bar{2}0)/Ni(111)$ interface systems obtains 1.53e, 1.36e and 1.15e charge, respectively. The above results indicate that there is a certain proportion of ionic bonds at the interface, and the ionic bond makes the interface more strongly bonded. The charge transfer amount at the $Si_3N_4(11\bar{2}0)/Ti(0001)$ interface is the largest, indicating that a stronger ionic bond is formed between the interface atoms, and the interface system is more stable.

Fig. 5(a) shows that the total density of states of N and Ti atoms is overlapped at −15 eV and in the −5 eV to 0 eV range, indicating that the electron orbit is hybridized. Fig. 5(b) shows that N-2p has different degrees of hybridization with Ti-3 s, Ti-3p, and Ti-3d orbitals, forming a covalent bond structure. The density of states indicates that there is not only electron transfer at $Si_3N_4(11\bar{2}0)/Ti(0001)$, but also orbital hybridization between N and Ti atoms. Therefore, the interface system not only forms an ionic bond, but also covalent bond, which further enhances the interfacial bond strength and facilitates the formation of a more stable structure. It can be seen from Fig. 5(c) that there is an identical peak between the N and Cr atoms, indicating that there is an overlap between the electron orbitals of the N and Cr atoms. Fig. 5(d) shows that the N atom N-2p and Cr atom Cr-3 s, Cr-3p, and Cr-3d orbitals have different degrees of hybridization, forming covalent bonds. Fig. 5 (e) shows that there is an overlap of electron clouds between N and Ni atoms, indicating the existence of electron orbital hybridization of N atoms and Ni. Fig. 5(f) shows that a covalent bond is formed because of the hybridization of N-2p with the Cr-3 s, Cr-3p, and Cr-3d orbitals.

The size of the overlapping area of the density of states can qualitatively judge the bond strength of the interface atoms [28]. Therefore, The overlapping area of the total density of states of three kinds of interfaces is calculated by integration, and the calculation results are

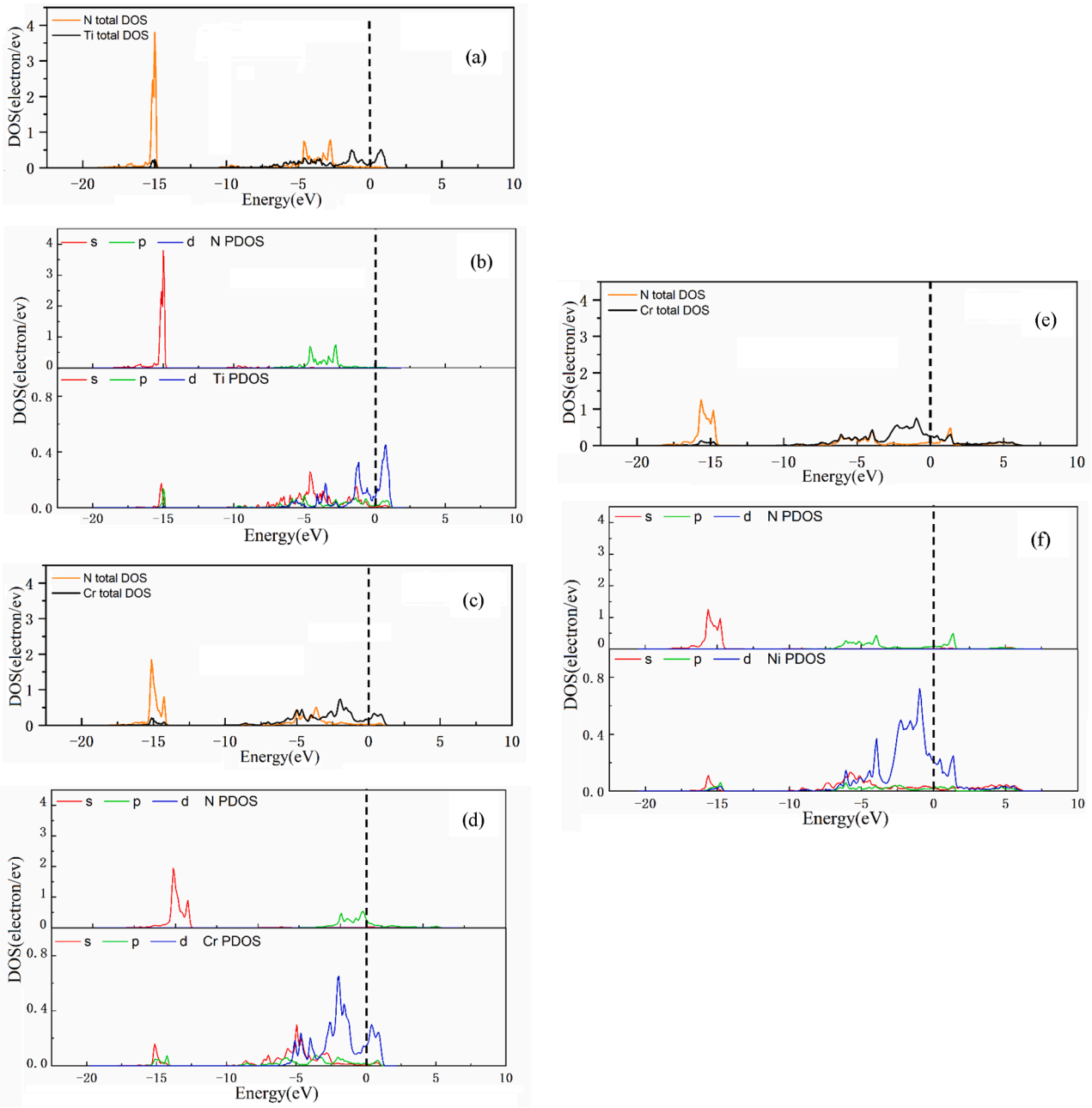

Fig. 5. (a) The total density of states of the $Si_3N_4(11\bar{2}0)$/Ti(0001) interface, (b) partial densities of states of the $Si_3N_4(11\bar{2}0)$/Ti(0001) interface, (c) total density of states of the $Si_3N_4(11\bar{2}0)$/Cr(110) interface, (d) partial densities of states of the $Si_3N_4(11\bar{2}0)$/Cr(110) interface, (e) total density of states of the $Si_3N_4(11\bar{2}0)$/Ni (111) interface, (f) partial densities of states of $Si_3N_4(11\bar{2}0)$/Ni(111) interface.

Table 7
Overlapping area in the total density of states diagram of interface system.

Interface	Overlapping area
$Si_3N_4(11\bar{2}0)$/Ti(0001)	0.885
$Si_3N_4(11\bar{2}0)$/Cr(110)	0.827
$Si_3N_4(11\bar{2}0)$/Ni(111)	0.861

shown in Table 7. It is found that there is little difference in the area of the overlap region between the three kinds of interface systems. The overlap area of $Si_3N_4(11\bar{2}0)$/Ti(0001) interface is the largest, indicating that the N-Ti covalent bond formed between N atoms and Ti atoms is slightly stronger than N-Cr bonds and N-Ni bonds. The overlap area of $Si_3N_4(11\bar{2}0)$/Ti(0001) interface is the largest, which indicates that the N-Ti covalent bond is slightly stronger than that of N-Cr bond and N-Ni bond. Combined with the Bader charge of the interface atom in Table 6, it shows that the bonding between N atoms and Ti atoms is stronger. Therefore, $Si_3N_4(11\bar{2}0)$/Ti(0001) is the best combination to construct Si_3N_4 ceramic/metal interface system.

4. Conclusions

The bonding at interfaces between Si_3N_4 ceramics and Ti, Cr and Ni metals was studied employing the first principles calculations based on the density functional theory. The optimized geometry, work of separation, electron density difference, the Bader charge and the density of

states for the interface models were calculated. The main results are summarized as follows:

(1) The close-packed surfaces of Ti, Cr, Ni, Ti (0001), Cr (1 1 0), Ni (1 1 1) have the lowest surface energy, and for the Si_3N_4 ceramics, the (1 1 $\bar{2}$ 0) surface has the lowest surface energy, indicating that it is more stable.
(2) The work of separation of the Si_3N_4(1 1 $\bar{2}$ 0)/Ti(0001), Si_3N_4(1 1 $\bar{2}$ 0)/Cr(1 1 0), and Si_3N_4(1 1 $\bar{2}$ 0)/Ni(1 1 1) interfaces is relatively large in a series of interface systems composed of the low-index crystal planes of Si_3N_4, Ti, Cr, and Ni. The Si_3N_4(1 1 $\bar{2}$ 0)/Ti(0001) interface has the largest separation work, which is the optimal combination of several Si_3N_4 ceramics and metal interface structures studied in this paper.
(3) The charge density difference results show that the charge of the Ti atom at the Si_3N_4(11$\bar{2}$0)/Ti(0001) interface shifts towards the N atom, and a strong bond is formed at the interface. The Bader charge result quantifies the charge transfer between the N atom and the metal atom at the interface. The Si_3N_4(11$\bar{2}$0)/Ti(0001) interface system has the largest amount of charge transfer, indicating that the electronic interaction of the interface system is stronger and thus a stronger bond is formed.
(4) The density of states reflects the orbital hybridization between the N atoms and Ti, Cr and Ni atoms at the interface. N-Ti, N-Cr, and N-Ni covalent bonds are formed at the interface, and the covalent bonds further enhance the atomic bonding at the interface. The covalent bond of the Si_3N_4(11$\bar{2}$0)/Ti(0001) interface is stronger. The above results indicate that Si_3N_4(11$\bar{2}$0)/Ti (0001) is the best choice for constructing the Si_3N_4/metal interface.

CRediT authorship contribution statement

Sen Yang: Software, Investigation, Writing - original draft, Writing - review & editing, Visualization. **Bingzheng Yang:** Conceptualization, Methodology, Writing - original draft. **Hao Ren:** Validation, Formal analysis. **Huisheng Yang:** Project administration, Resources, Writing - original draft. **Xiaolu Pang:** Resources, Supervision, Writing - review & editing. **Kewei Gao:** Project administration, Supervision. **Alex A. Volinsky:** Writing - original draft.

Declaration of Competing Interest

The authors declare that they have no known competing financial interests or personal relationships that could have appeared to influence the work reported in this paper.

Acknowledgments

This work was supported by the National Natural Science Foundation of China (No. 51771025, 51922002).

References

[1] K. Rahim, and A. Mian, A review on laser processing in electronic and MEMS packaging, J Electron. Packaging. 139(3) (2017).
[2] T. Ahsan, A. Schoenberg, Investigation of the Mechanisms of Adhesion and Failure in Microelectronic Packages, Adhesion In Microelectronics (2014) 313–341.
[3] P. Baracchini, C. Guillebaud, F.X. Kromm, H. Wargnier, Multi-material Design in the Case of a Coupled Selection of Architectures and Materials: Application to Embedded Electronic Packaging, J. Mater. Eng. Perform. 28 (12) (2019) 7248–7258.
[4] F. Lang, H. Yamaguchi, H. Nakagawa, H. Sato, Cyclic Thermal Stress-Induced Degradation of Cu Metallization on Si_3N_4 Substrate at−40°C to 300°C, J. Electron. Mater. 44 (1) (2015) 482–489.
[5] H. Okumura, Present status and future prospect of widegap semiconductor high-power devices, Jpn. J. Appl. Phys. 45(10R)(2006)7565.
[6] C.R. Eddy, D.K. Gaskill, Silicon carbide as a platform for power electronics, Science. 324 (5933) (2009) 1398–1400.
[7] Y. Zhou, H. Hyuga, D. Kusano, Y.I. Yoshizawa, K. Hirao, A tough silicon nitride ceramic with high thermal conductivity, Adv. Mater. 23 (39) (2011) 4563–4567.
[8] P. Ning, R. Lai, D. Huff, F. Wang, K.D. Ngo, V.D. Immanuel, K.J. Karimi, SiC wirebond multichip phase-leg module packaging design and testing for harsh environment, IEEE. T. Power. Electr. 25 (1) (2009) 16–23.
[9] R. Khazaka, L. Mendizabal, D. Henry, R. Hanna, Survey of high-temperature reliability of power electronics packaging components, IEEE. T. power. Electr. 30 (5) (2014) 2456–2464.
[10] L. Dupont, Z. Khatir, S. Lefebvre, S. Bontemps, Effects of metallization thickness of ceramic substrates on the reliability of power assemblies under high temperature cycling, Microelectron. Reliab. 46 (9) (2006) 1766–1771.
[11] Y. Yoshino, H. Ohtsu, T. Shibata, Thermally induced failure of copper-bonded alumina substrates for electronic packaging, J. Am. Ceram. Soc. 75 (12) (1992) 3353–3357.
[12] S. Hampshire, H.K. Park, D.P. Thompson, K. Jack, α′-Sialon ceramics, Nature. 274 (5674) (1978) 880–882.
[13] T.G. Lei, J.N. Calata, K.D.T. Ngo, G.Q. Lu, Effects of large-temperature cycling range on direct bond aluminum substrate, IEEE Transactions on Device and Materials Reliability. 9 (4) (2009) 563–568.
[14] J.S. Haggerty, A. Lightfoot, Opportunities for Enhancing the Thermal Conductivities of SiC and Si_3N_4 Ceramics Through Improved Processing, Ceramic Engineering and Science Proceedings. 475–487 (1995).
[15] N. Hirosaki, S. Ogata, C. Kocer, H. Kitagawa and Y. Nakamura, Molecular dynamics calculation of the ideal thermal conductivity of single-crystal α-and β−Si3N4, Phys. Rev. B. 65(13)(2002)134110.
[16] T. Funaki, A. Nishio, T. Kimoto, T. Hikihara, A study on electro thermal response of SiC power module during high temperature operation, IEICE Electronics Express. 5 (16) (2008) 597–602.
[17] Y. Zhou, H. Hyuga, D. Kusano, Y.I. Yoshizawa, T. Ohji, K. Hirao, Development of high-thermal-conductivity silicon nitride ceramics, J Asian Ceram Soc. 3 (3) (2015) 221–229.
[18] R.L. Mehan, D.W. McKee, Interaction of metals and alloys with silicon-based ceramics, J. Mater. Sci. 11 (6) (1976) 1009–1018.
[19] H.K. Lee, J.Y. Lee, Decomposition and interfacial reaction in brazing of SiC by copper-based active alloys, J. Mater. Sci Lett. 11 (9) (1992) 550–553.
[20] J.K. Boadi, T. Yang, T. Iseki, Brazing of pressureless-sintered SiC using Ag-Cu-Ti alloy, J. Mater. Sci Lett. 22 (7) (1987) 2431–2434.
[21] K. Nogi, Wetting phenomena at high temperature (Part III), Transactions of JWRI.22(2)(1993)183-188.
[22] Y. Zhao, H. Bian, W. Fu, Y. Hu, X. Song, D. Liu, Laser-induced metallization of porous Si_3N_4 ceramic and its brazing to TiAl alloy, J. Am. Ceram. Soc. 102 (1) (2019) 32–36.
[23] H.C. Chia, C.L. Chien, Microstructural Development of the AlN/Ti Diffusion Couple Annealed at 1000 °C, J. Am. Ceram. Soc. 91 (4) (2008) 1273–1280.
[24] W.B. Hanson, K.I. Ironside, J.A. Fernie, Active metal brazing of zirconia, Acta Mater. 48 (18) (2000) 4673–4676.
[25] A. Fukumoto, D. Berry, K.D.T. Ngo, G.Q. Lu, Effects of Extreme Temperature Swings (-55°C to 250°C) on Silicon Nitride Active Metal Brazing Substrates, IEEE Transactions on Device and Materials Reliability. 14 (2) (2014) 751–756.
[26] N. Murayama, K. Hirao, M. Sando, T. Tsuchiya, H. Yamaguchi, High-temperature electro-ceramics and their application to SiC power modules, Ceram. Int. 44 (4) (2018) 3523–3530.
[27] M. Goetz, N. Kuhn, B. Lehmeier, A. Meyer, U. Voeller, Comparison of silicon nitride DBC and AMB substrates for different applications in power electronics, PCIM Europe Conference Proceeding, *Power Electronics Conference PCIM*. 1 (2013) 57–65.
[28] L.M. Liu, S.Q. Wang, and H.Q. Ye, Adhesion of metal–carbide/nitride interfaces: Al/TiC and Al/TiN, J Phys: Condens. Mat. 15(47)(2003)8103.
[29] Z. Lin, X. Peng, T. Fu, Y. Zhao, C. Feng, Huang, and Z. Wang, Atomic structures and electronic properties of interfaces between aluminum and carbides/nitrides: A first-principles study, Physica. E. 89(2017)15-20.
[30] Y. Tao, G. Ke, Y. Xie, Y. Chen, S. Shi, H. Guo, Adhesion strength and nucleation thermodynamics of four metals (Al, Cu, Ti, Zr) on AlN substrates, Appl. Surf. Sci. 357 (2015) 8–13.
[31] W. Jin, L. Li, S. Zhang, H. Yang, K. Gao, X. Pang, A.A. Volinsky, First principles calculations of interfacial properties and electronic structure of the AlN (0 0 0 1)/Ti (0 0 0 1) interface, Chem Phys Lett 713 (2018) 153–159.
[32] D.J. Siegel, L.G. Jr Hector, and J. B. Adams, Ab initio study of Al-ceramic interfacial adhesion, Phys. Rev. B. 67(9)(2003)092105.
[33] G. Kresse, J. Hafner, Ab initio molecular dynamics for liquid metals. Phys Rev B Condens Matter, Phys. Rev. B. 48 (17) (1993) 13115–13118.
[34] G. Kresse, Efficient iterative schemes for ab initio total-energy calculations using a plane-wave basis set, Phys. Rev. B. 54 (16) (1996) 11169–11186.
[35] A.K. Rajagopal, J. Callaway, Electron Gas, Phys. Rev. 7 (5) (1973) 864–871.
[36] J.P. Perdew, K. Burke, Y. Wang, Generalized gradient approximation for the exchange-correlation hole of a many-electron system, Phys. Rev. B. 54 (23) (1996) 16533–16539.
[37] J.P. Perdew, K. Burke, M. Ernzerhof, Generalized Gradient Approximation Made Simple, Phys. Rev. Lett. 77 (18) (1996) 3865–3868.
[38] J.D. Pack, H.J. Monkhorst, Special points for Brillouin-zone integrations—a reply, Phys. Rev. B. 16 (4) (1977) 1748–1749.
[39] M.Yang, R.Q. Wu, W.S. Deng, L. Shen, Z.D. Sha, Y.Q. Cai, and S.J. Wang, Electronic structures of B-Si3N4 (0001) /Si (111) interfaces: Perfect bonding and dangling bond effects, J. Appl. Phys. 105(2)(2009)024108.

[40] A.Y. Kuksin, A.S. Rokhmanenkov, V.V. Stegailov, Atomic positions and diffusion paths of h and he in the α-Ti lattice, Phys. Solid. State. 55 (2) (2013) 367–372.
[41] R.Soulairol, C.C. Fu, and C. Barreteau, Magnetic and energetic properties of low-index Cr surfaces and Fe/Cr interfaces: A first-principles study, Phys. Rev. B. 84 (15)(2011)155402.
[42] P. Peng, Z.H. Jin, R. Yang, Z.Q. Hu, First principles study of effect of lattice misfit on the bonding strength of Ni/Ni3Al interface, J. Mater. Sci. 39 (12) (2004) 3957–3963.
[43] R. Tran, Z. Xu, B. Radhakrishnan, D. Winston, W. Sun, K.A. Persson, S.P. Ong, Surface energies of elemental crystals, Scientific Data, *Sci. Data.* 3 (1) (2016) 1–13.
[44] M. Böhringer, P. Molinas-Mata, E.Artacho, and J. Zegenhagen, Surface energy and stability of stress-driven discommensurate surface structures, Phys. Rev. B. 52(23) (1995)16373.
[45] S.D. Waele, K. Lejaeghere, M. Sluydts, and S. Cottenier, Error estimates for density-functional theory predictions of surface energy and work function, Phys. Rev. B. 94 (23)(2016)235418.
[46] W. Li, L. Huang, R.G.S. Pala, G.H.Lu, F. Liu, J.W. Evans, and Y. Han, Thickness-dependent energetics for Pb adatoms on low-index Pb nanofilm surfaces: First-principles calculations, PPhys. Rev. B. 96(20)(2017)205409.
[47] L. Vitos, A.V. Ruban, H.L. Skriver, J. Kollar, The surface energy of metals, Surf Sci. 411 (1–2) (1998) 86–202.
[48] J. Wellendorff, K.T. Lundgaard, A. Møgelhøj, V. Petzold, D.D. Landis, J.K. Nørskov, T. Bligaard and K.W. Jacobsen,. Density functionals for surface science: Exchange-correlation model development with Bayesian error estimation, Phys Rev B. 85(23) (2012)235149.
[49] D.F. Johnson, E.A. Carter, Bonding and Adhesion at the SiC/Fe Interface, J. Phys. Chem. A. 113 (16) (2009) 4367–4373.
[50] S.Lu, Q.M Hu, R. Yang, B. Johansson, and L. Vitos, First-principles determination of the alpha-alpha' interfacial energy in Fe-Cr alloys, Phys. Rev. B. 82(2010)195103.
[51] E.T. Dong, P. Shen, L.X. Shi, D. Zhang, Q.C. Jiang, Wetting and adhesion at Mg/MgO interfaces, J Mater Sci. 48 (17) (2013) 6008–6017.
[52] X.Y. Xu, H.Y. Wang, M. Zha, C. Wang, Z.Z. Yang, Q.C. Jiang, Effects of Ti, Si, Mg and Cu additions on interfacial properties and electronic structure of Al(111)/4H-SiC(0001) interface: A first-principles study, Appl. Surf. Sci. 437 (2018) 103–109.
[53] S.V. Dudiy, B.I. Lundqvist, First-principles density-functional study of metal-carbonitride interface adhesion: Co/TiC(001) and Co/TiN(001), Phys. Rev. B. 64 (4) (2001) 314–319.
[54] N. Jin, Y. Yang, X. Luo, J. Li, B. Huang, S. Liu, Z. Xiao, Theoretical calculations on the adhesion, stability, electronic structure and bonding of SiC/W interface, Appl. Surf. Sci. 314 (2014) 896–905.
[55] G. Barcaro, L. Sementa, F.R. Negreiros, A. Fortunelli, Influence of temperature and H 2 adsorption on the structure of silica-supported gold subnanometer clusters, Comput. Theor. Chem. 1021 (2013) 222–228.
[56] G.C. Ma, J.L. Fan, and H.R. Gong, Fundamental effects of hydrogen on cohesion properties of Cu/W interfaces. Solid State Communications, Solid. State. Commun. 250(2017)79-83.